Article

Observation of chiral state transfer without encircling an exceptional point

https://doi.org/10.1038/s41586-022-04542-2

Received: 30 September 2021

Accepted: 14 February 2022

Published online: 11 May 2022

Check for updates

Hadiseh Nasari[1,2], Gisela Lopez-Galmiche[2], Helena E. Lopez-Aviles[2], Alexander Schumer[1,3], Absar U. Hassan[2], Qi Zhong[2], Stefan Rotter[3], Patrick LiKamWa[2], Demetrios N. Christodoulides[2] & Mercedeh Khajavikhan[1,4]✉

The adiabatic theorem, a corollary of the Schrödinger equation, manifests itself in a profoundly different way in non-Hermitian arrangements, resulting in counterintuitive state transfer schemes that have no counterpart in closed quantum systems. In particular, the dynamical encirclement of exceptional points (EPs) in parameter space has been shown to lead to a chiral phase accumulation, non-adiabatic jumps and topological mode conversion[1–8]. Recent theoretical studies, however, have shown that contrary to previously established demonstrations, this behaviour is not strictly a result of winding around a non-Hermitian degeneracy[9]. Instead, it seems to be mostly attributed to the non-trivial landscape of the Riemann surfaces, sometimes because of the presence of an EP in the vicinity[9–11]. Here, in an effort to bring this counterintuitive aspect of non-Hermitian systems to light and confirm this hypothesis, we provide a set of experiments to directly observe the field evolution and chiral state conversion in an EP-excluding cycle in a slowly varying non-Hermitian system. To do so, a versatile yet unique fibre-based photonic emulator is realized that utilizes the polarization degrees of freedom in a quasi-common-path single-ring arrangement. Our observations may open up new avenues for light manipulation and state conversion, as well as providing a foundation for understanding the intricacies of the adiabatic theorem in non-Hermitian systems.

The energy Riemann surfaces associated with non-Hermitian Hamiltonians exhibit a complex non-trivial topology that is strongly affected by the presence of non-Hermitian degeneracies[12–19]. This is shown to enable non-trivial state transfer dynamics in slowly evolving non-Hermitian systems when an EP is encircled[1–11,20–24]. For example, experimental works in two-state exciton-polariton systems[25] and in microwave cavities[26] show that winding around an EP under quasi-static conditions leads to a mode exchange occurring at the end of a parametric loop, accompanied by an effective geometric phase of π for one of the modes[27–29]. For a fully dynamical loop around an EP, the contribution of non-Hermiticity and its inevitable concomitant, (namely non-adiabatic) transitions gives rise to a fundamentally different chiral behaviour. In this case, if the encirclement is carried out in a clockwise (CW) fashion, for any arbitrary input that happens to be a mixture of the two eigenstates, the system always ends in one of the eigenmodes. On the other hand, if the loop is traversed in the opposite direction (that is, in an anticlockwise (ACW) manner), the second eigenstate is robustly produced, irrespective of the input state composition[1–11,20–24]. Analytical studies using confluent hypergeometric functions provide a way to justify this marked behaviour[7,9]. In the past few years, dynamical EP encirclement and the ensuing mode conversion have been reported in lossy microwave waveguide arrangements with a judiciously patterned boundary modulation[4,11], in cryogenic optomechanical oscillators[5] and in silicon photonic-based optical waveguides[6]. Finally, although remarkable progress has been made in monitoring the field intensities of radiofrequency signals during the encirclement process[24], a direct observation of the evolution of the full state of light in these dynamical systems is still lacking.

Recent theoretical studies, however, have challenged these findings by showing that the counterintuitive chiral state transfer in these systems is not necessarily associated with encircling an EP[9–11]. Instead, the topology and landscape of the intersecting Riemann surfaces and the trajectory and speed of the steering process greatly influence the outcome of a parametric loop. For example, without strictly winding an EP, one may still be able to observe a chiral behaviour, or dynamically encircling an EP along two dissimilar paths in the parameter space may result in different outputs when multiple EPs are involved[9–11,30]. In this Article, we report on directly probing the temporal evolution of light in systems with slowly varying non-Hermitian Hamiltonians in order to render a more complete portrait of the physics of quasi-adiabatic steering. In particular, we monitor the polarization state of a laser pulse on the Poincaré sphere as it circulates in a time-varying fibre ring. By imposing intensity and phase modulation as well as polarization mixing, each round trip in the ring effectively represents a new point in the parameter space. Consequently, a judicious modulation pattern over consecutive round trips allows the system to emulate an arbitrary parametric loop.

[1]Ming Hsieh Department of Electrical and Computer Engineering, University of Southern California, Los Angeles, CA, USA. [2]CREOL, The College of Optics & Photonics, University of Central Florida, Orlando, FL, USA. [3]Institute for Theoretical Physics, Vienna University of Technology (TU Wien), Vienna, Austria. [4]Department of Physics & Astronomy, University of Southern California, Los Angeles, CA, USA. ✉e-mail: khajavik@usc.edu

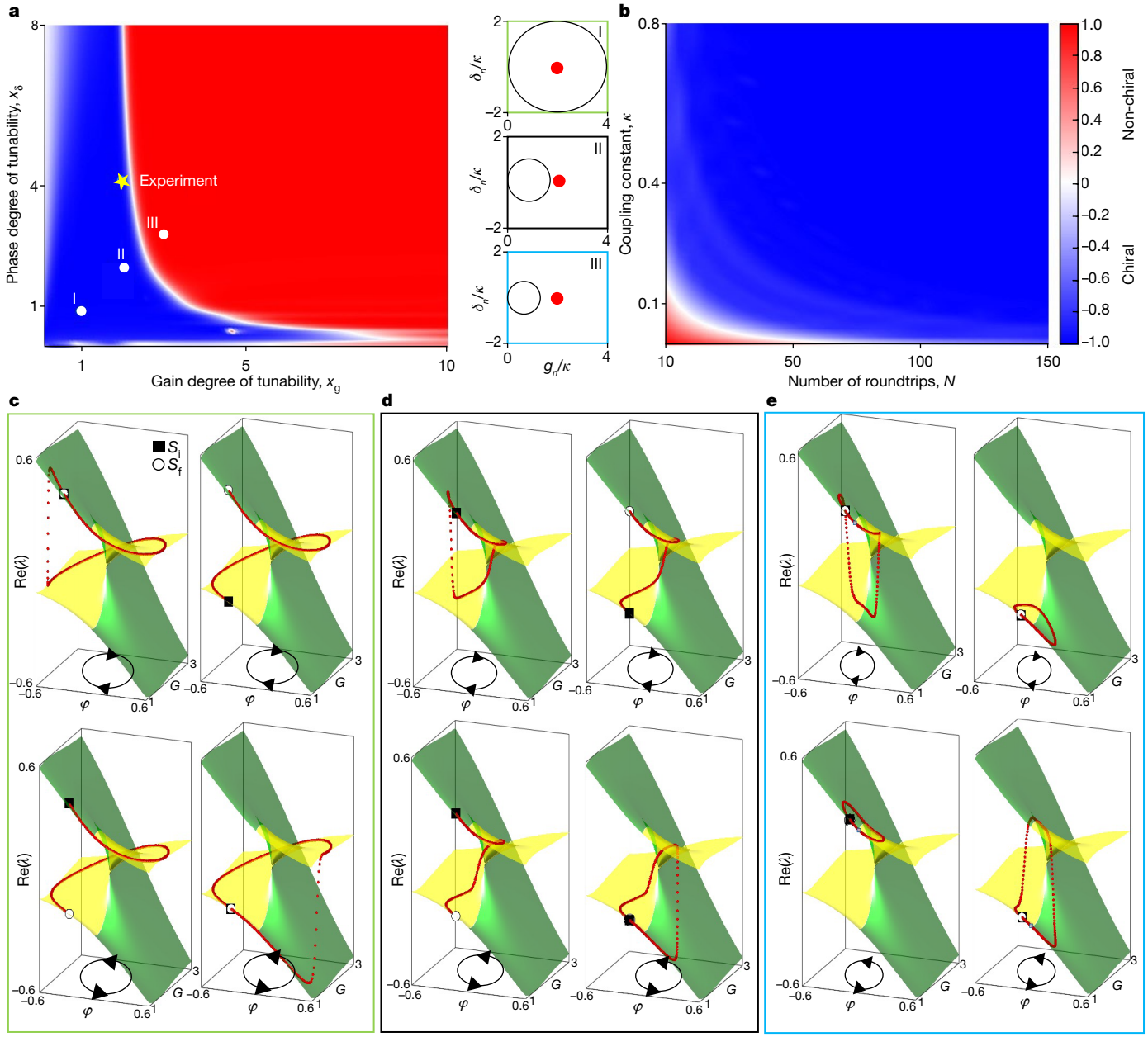

Fig. 1 | Self-intersecting Riemann manifolds in the gain-phase parameter space and chiral mode conversion. a, A quantitative insight into the chirality of parametric steering of a Hamiltonian in the vicinity of a non-Hermitian singularity, performed through trajectories defined by $\delta_n = 2\kappa\rho x_\delta^{-1}\sin(\gamma 2\pi n/N)$ and $g_n = 2\kappa x_g^{-1}[1-\rho\cos(\gamma 2\pi n/N)]$ with $N = 50$, $\kappa = 0.7$, $\rho = 1$, in which x_g and x_δ represent tunable gain and phase parameters. For a given set of parameters (x_g, x_δ), blue indicates a loop with a chiral response, whereas red denotes a non-chiral result. **b**, Adiabaticity as a prerequisite for a parametric loop sets a lower limit on the coupling strength between the two perpendicular polarization components and the number of round trips. The chirality map shown here elucidates this limit for the case $x_g = x_\delta = 2.05$. **c**, Here we numerically explain the chirality exhibited by the dynamic variation of a non-Hermitian Hamiltonian in the gain-phase parameter space $[G = \exp(g_n), \varphi = \delta_n]$ through the trajectories defined by equation (2) for $N = 300$, $\kappa = 0.3$, $\rho = 1$, $x_g = 1$ and $x_\delta = 1$ (red dots), when initiated from each polarization eigenstate on either of the Riemann surfaces (denoted as S_i and marked by a black square), for both CW and ACW encirclement helicities ($\gamma = \pm 1$, indicated by the black arrows underneath). The light's polarization evolves towards an eigenstate of the system, locked to the sense of rotation, no matter what the initial state is. The final state is indicated by S_f and is represented by a white circle. **d**, **e**, The same as **c**, but when the EP is not included in the parametric loop. In **d**, the EP still lies in the vicinity of the loop whereas in **e** it is positioned far away. Red dots in **c**–**e**, numerically obtained by solving the difference equation (Supplementary equation (3)) and the consecutive projection of the dynamical evolution onto the Riemann surfaces through $[\mathrm{Re}(\lambda_1(t))|c_1(t)|^2 + \mathrm{Re}(\lambda_2(t))|c_2(t)|^2]/[|c_1(t)|^2 + |c_2(t)|^2]$, represent the evolution of the eigenvalues of the system during the parametric steering process (Supplementary Section 2). The underlying Riemann surfaces are associated with the real part of the eigenvalues of the corresponding Hamiltonian of the system with the green and yellow colour indicating (relative) loss and gain, respectively.

We note that this approach is different from that used with standard spatially non-uniform coupled waveguide systems for which information about the state of light is available only at the input and output ports. Instead, through this unique arrangement, we are able to observe the light's full state evolution as it undergoes adiabatic transformations and non-adiabatic jumps in the vicinity of an EP without encircling it.

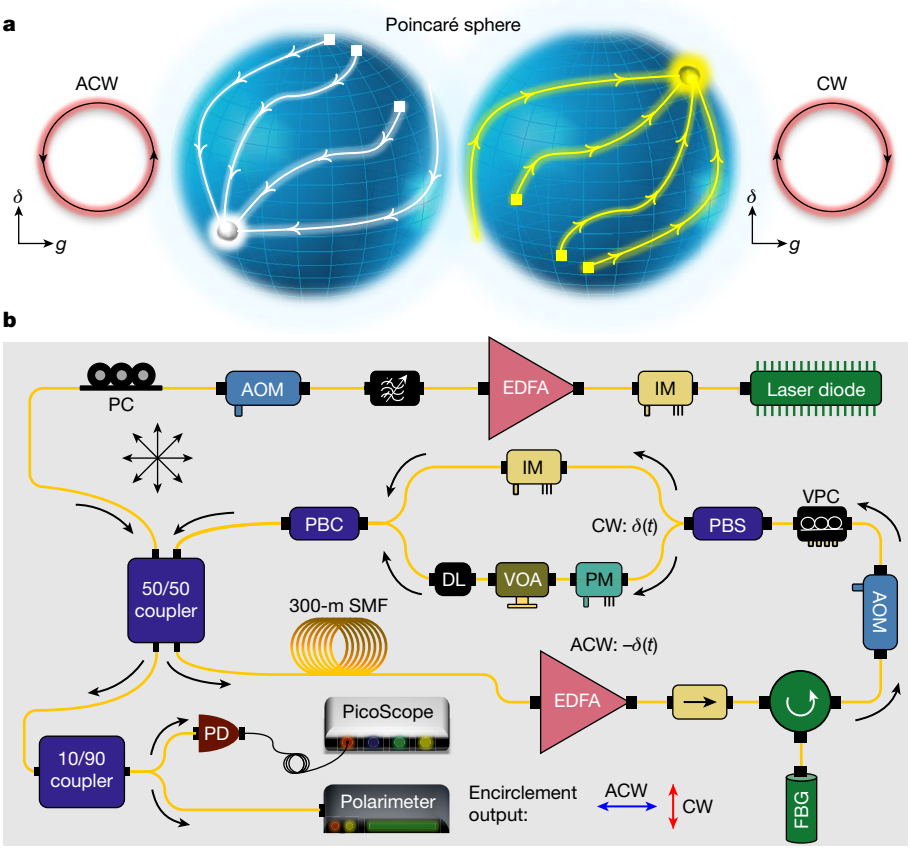

Fig. 2 | Operation principle of the devised fibre-based photonic emulator. a, Conceptual illustration of the chiral mode conversion in the polarization domain as a result of dynamic steering of a non-Hermitian Hamiltonian around its singularity in parameter space. The polarization is funnelled into one of the orthogonal eigenstates of the system and is solely determined by the helicity of the parametric loop. **b**, Experimental setup. The seed pulse module is composed of a laser diode and an intensity modulator (IM) for generating pulses, an erbium-doped fibre amplifier (EDFA) for pulse amplification, an acousto-optic modulator (AOM), a tunable bandpass filter for removing the excess noise introduced by the EDFA, and a polarization controller (PC) for adjusting the initial polarization state. A 300-m long single-mode fibre (SMF) sets the pulse round-trip time and the AOM acts as a gate, controlling the number of round trips (Supplementary Section 3). The variable polarization controller (VPC) calibrates the setup and couples the polarization components. The desired gain-phase variation of the two polarizations is realized by using a polarization beamsplitter (PBS), an intensity modulator, a phase modulator (PM), a delay line (DL), a variable optical attenuator (VOA), and a polarization beam combiner (PBC). The fibre Bragg grating (FBG) removes the pilot wavelength after the EDFA and purifies the signal from any amplified spontaneous emission noise from the EDFA. At the end of each round trip, half of the pulse is routed to a monitoring module, equipped with an InGaAs photo detector (PD), a PicoScope and a polarimeter, and the other half is launched back into the fibre loop for recirculation at predetermined times.

In our study, the dynamics of the time-varying light propagation process is governed by a discrete analogue of the Schrödinger equation $|\psi_{n+1}\rangle = (1 - iH_n)|\psi_n\rangle$, in which $|\psi_n\rangle = [a_n, b_n]^T$ is the Jones vector representation of the polarization state with field amplitudes a_n and b_n at the n th round trip (Supplementary Section 1). The associated binary non-Hermitian Hamiltonian corresponding to the nth circulation in the fibre is given by

$$H_n = \begin{pmatrix} ig_n & \kappa \\ \kappa & \delta_n \end{pmatrix}, \qquad (1)$$

in which κ denotes a fixed coupling strength between the two orthogonal polarization constituents. Unlike in strict parity–time (PT)-symmetric configurations with traceless Hamiltonians, here we have an unbalanced arrangement, in which one of the two polarization components (a_n) is subject to a round-trip-dependent gain g_n and the other (b_n) is subject to a detuning δ_n (phase mismatch). Clearly, for a parametric configuration of $\delta = 0$ and $g = 2\kappa$, the requirement for the emergence of a second-order EP is met (in almost a PT-symmetric configuration[15,17,18]). The quasi-adiabatic steering of the Hamiltonian in the gain-detuning parameter space can be achieved by establishing (discrete) temporal profiles for both the phase and gain as follows:

$$\delta_n = 2\kappa\rho x_\delta^{-1}\sin(\gamma 2\pi n/N)\; g_n = 2\kappa x_g^{-1}[1 - \rho\cos(\gamma 2\pi n/N)], \qquad (2)$$

in which x_g and x_δ are gain and phase tuning parameters, and ρ signifies the radius of a closed circular contour when $x_g = x_\delta$ (Fig. 1a). The choice of these parameters determines the shape of the parametric path. The direction of encirclement in equation (2) is dictated by the binary variable γ; for $\gamma = 1$, a CW EP encirclement is executed, and $\gamma = -1$ leads to a ACW loop. The total number of round trips of the light pulse in the fibre ring, indicated by N in equation (2), introduces a tunable degree of freedom to control the rate of change in gain and detuning after each cycle and thus the adiabaticity of the encirclement process. The onset of the dynamical encirclement lies in the PT-unbroken phase to warrant a chiral response while avoiding unstable/undetectable modes (as a consequence of optical amplification/decay in the PT-symmetry-broken phase[17,18]).

Figure 1a illustrates the effect of the position of the parametric loop on the chiral mode conversion behaviour. As can be seen, the directional response can still be observed even if the contour does not include an EP, provided that the winding is carried out sufficiently close to the EP and in a quasi-adiabatic manner[9]. Importantly, it shows that the chirality of mode conversion depends on the geometry of the parametric trajectories when the EP is not encircled. The degree of adiabaticity can be controlled by adjusting the coupling strength and the number of round trips N, which in turn affects the chirality of the process. These parameters can be modified at will to manipulate both the shape and relative position of the parametric loop with respect to the EP (Fig. 1b and Supplementary Section 2). The quantity that measures the relative distribution of the eigenstate amplitudes over time is the eigenstate population $p(t) = [|c_1(t)|^2 - |c_2(t)|^2]/[|c_1(t)|^2 + |c_2(t)|^2]$. In this respect, p refers to the relative weight of the eigenvector coefficients $c_1(t)$ and $c_2(t)$ associated with the state vector $|\psi(t)\rangle$ expanded in an eigenbasis, here the eigenvectors of the Hamiltonian at the onset of the parametric steering process (that is, $|\psi(t)\rangle = c_1(t)|V_1\rangle + c_2(t)|V_2\rangle$). Evidently, this relative population lies in the range $p \in [-1,1]$. The product of the relative eigenstate populations of the CW and ACW directions, $p_{CW}p_{ACW}$, provides a way to quantify the chirality of a parametric path, as depicted in Fig. 1a, b. In this way, a chirality function can be defined as $\chi = p_{CW}p_{ACW}$, which also takes values in the range $\chi \in [-1,1]$.

The contribution of the complex topology of the Riemann energy manifolds is brought to the fore in Fig. 1c–e. For a loop centred at an EP

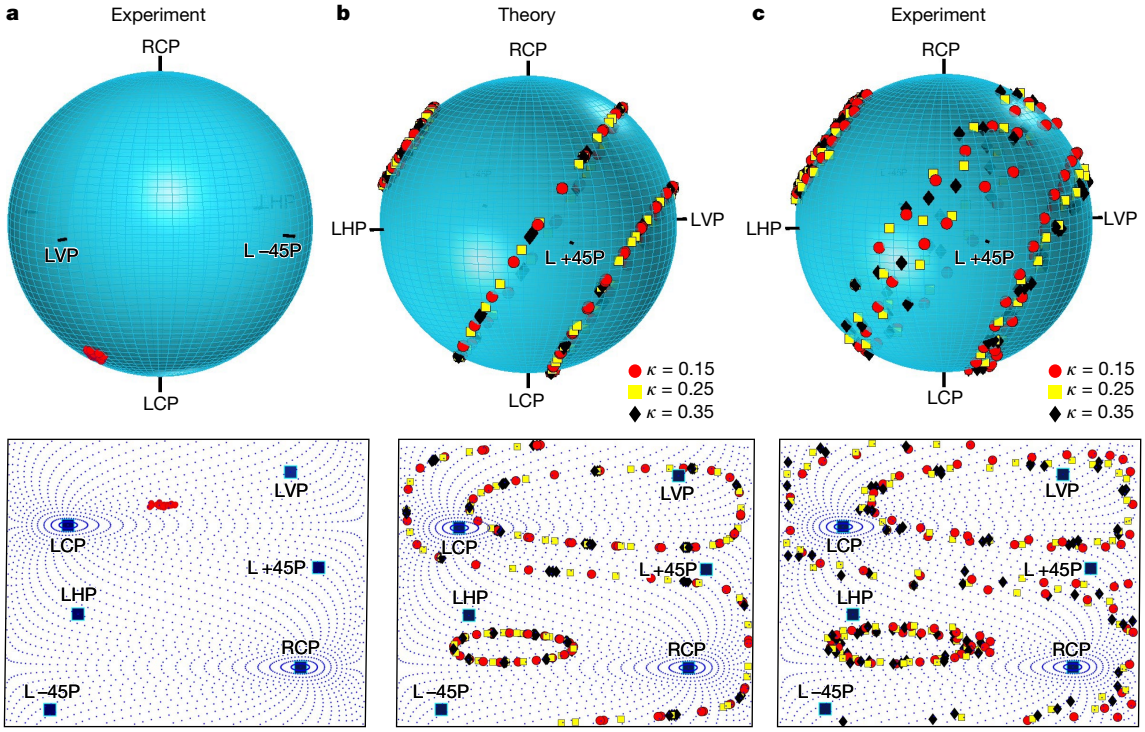

Fig. 3 | Polarization stability and coupling between the polarization components of a light pulse. a, Demonstrating the stability of the light pulse's polarization state over the probed time span of the experiment (over 50 round trips of the pulse in the fibre loop: 91.5 µs), when the polarization components are uncoupled and the intensity and phase modulators are deactivated. The polarization of the light at the end of each round trip (shown by red circles) has remained localized on the Poincaré sphere. This step is critical given that this fibre-based emulator is interferometric in nature and is thus susceptible to noise sources. LCP, left-handed circular polarization; RCP, right-handed circular polarization; LHP, linear horizontal polarization; LVP, linear vertical polarization; L +45P, linear +45° polarization; L −45P, linear −45° polarization **b**, **c**, Stokes vector representation of the polarization evolution of a light pulse when its polarization components are coupled to each other at a fixed strength. In this case, irrespective of the coupling level and initial conditions, the polarization state should move on circular trajectories on the Poincaré sphere that share the same axis of rotation, as also confirmed in the experiment. The end points of this axis represent the polarization eigenstates of the system. Theoretical simulations in **b** are in good agreement with the experimental results in **c**.

(Fig. 1c) and starting from one eigenstate, an encirclement direction towards the amplified state (yellow plane) yields an adiabatic process and a state flip occurs. However, for the opposite direction, for which the system initially tends to evolve with no amplification (green plane), the resulting non-adiabatic jump, a direct byproduct of the skewed vector space, returns the system to the initial eigenstate. These trajectories elucidate the fact that regardless of the initial state, the system always moves faithfully towards an eigenstate mandated by the direction of encirclement. Figure 1d shows that even by excluding the EP from this single-cycle parametric loop, the chirality of the process can still be retained depending on the proximity of the loop to the EP, provided that the Hamiltonian varies in a smooth fashion. Notably, to maintain the chiral state transfer, the field experiences a further non-adiabatic jump likewise in both directions and for both initial states. On the other hand, shifting the trajectory further away from the EP (Fig. 1e) can deteriorate the chiral behaviour.

A chiral mode conversion mechanism in the polarization domain can be viewed as an omni-polarizer action (Fig. 2a). Depending on a CW or an ACW encirclement, any random input polarization state will arrive at one of the two diametrical (antipodal) points on the Poincaré sphere that represent the two mutually orthogonal eigenstates of the system. The operation principle of our proposed photonic emulator is schematically described in Fig. 2b (Methods).

Of great importance in our experiments are the temporal and spatial stability of polarization states. A variable electrical polarization controller compensates the residual delay and ensures that the Mueller transfer function of the fibre loop is equal to the identity matrix. In addition, a soundproof box around the fibre loop shields the system from the effect of acoustic noise disturbances, and a judicious selection and configuration of the incorporated electro-optic and fibre devices establish the adequate steadiness to perform the experiments. First, to confirm the stability of the setup, we measure the polarization state of a pulse during 50 round trips in the absence of intensity and phase tuning. Figure 3a shows that without polarization-dependent modulations the polarization remains the same, indicating that the system is indeed governed by the identity Mueller transfer matrix. A crucial part of this setup is the coupling between the two polarization components. Using a polarization controller, the constant coupling κ is implemented through the induced retardation given that $\Gamma = 2\kappa$ (Supplementary Section 1). The effect of coupling was measured by examining the trajectory of the Stokes parameters of each pulse when three different initial states [$S_i^{(I)} = (-0.099, 0.24, -0.96)$, $S_i^{(II)} = (0.77, 0.55, -0.32)$ $S_i^{(III)} = (0.93, -0.14, 0.33)$] are probed on the Poincaré sphere with corresponding coupling levels $\kappa = 0.15, 0.25, 0.35$. Figure 3b, c compares the theoretically anticipated trajectories with those observed in the experiment. Note that the axis of rotation of the emerging circular trajectories remains constant under the exerted coupling strengths. Identifying this axis is important as its intersections with the Poincaré sphere reveal the two polarization eigenstates of the system.

Once stability is established, the parameter cycle is implemented by imposing the time-dependent phase and amplitude modulation (as stated in equation (2)). Generally, for a 50-cycle loop (91.5 µs duration) a coupling of $\kappa \approx 0.7$ is required to ensure that the condition for

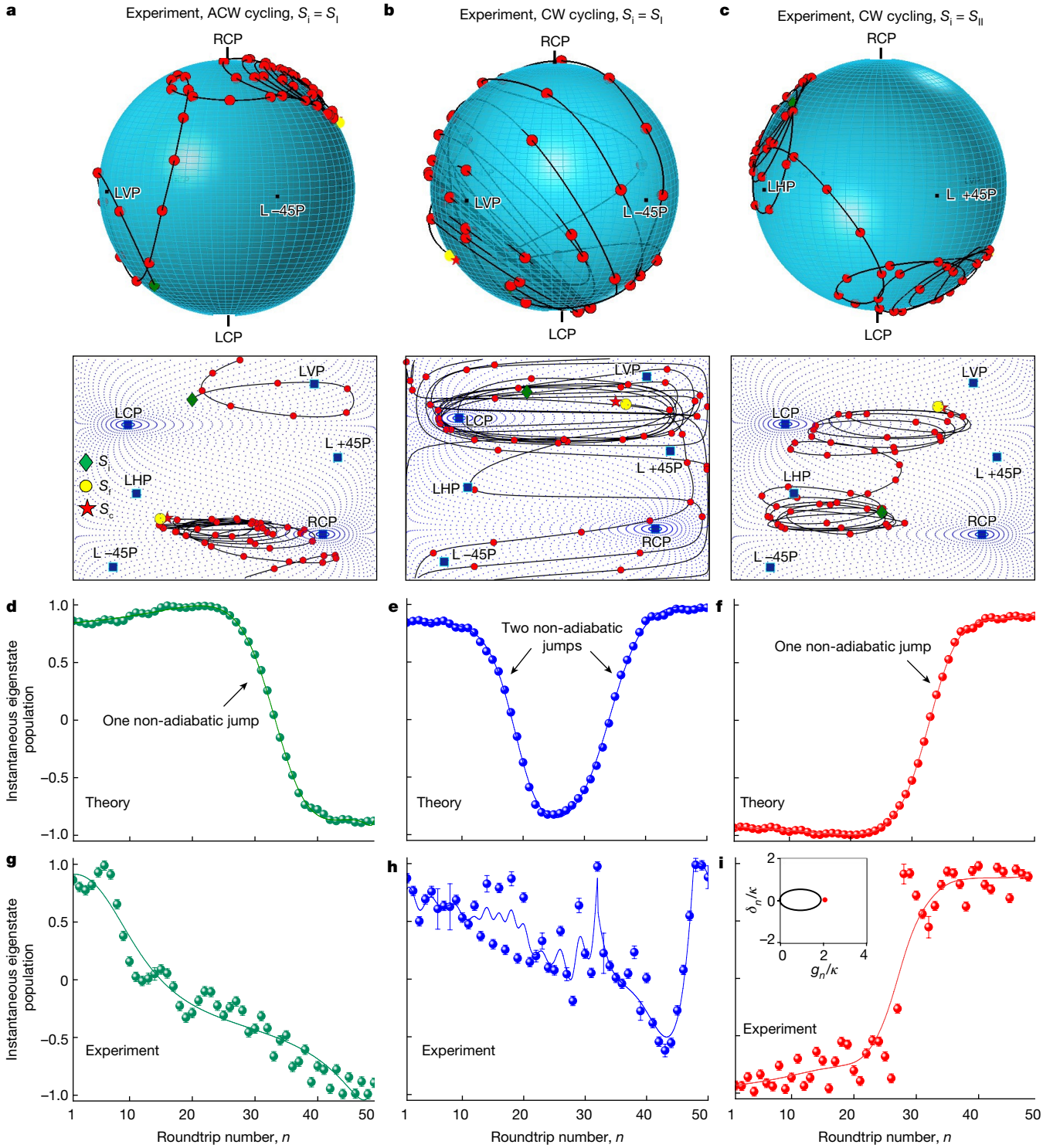

Fig. 4 | Experimental observation of chiral mode conversion through a parametric steering of the Hamiltonian along a trajectory that lies in the proximity of an EP. a, The system is excited with a light pulse that is an arbitrary mixture of the polarization eigenstates, denoted as S_i and shown by the green diamond, which happens to be close to the first eigenstate $|V_1\rangle$ of the Hamiltonian. This state is forced to traverse an EP-excluding parametric loop, albeit in its vicinity, in the gain-phase parameter space, characterized by the modulation patterns $\delta_n = 2\kappa\rho x_\delta^{-1}\sin(\gamma 2\pi n/N)$, $g_n = 2\kappa x_g^{-1}[1-\rho\cos(\gamma 2\pi n/N)]$ with $x_g = 2.04$ and $x_\delta = 4.2$. This loop is carried out in the ACW direction ($\gamma = -1$), through 50 round trips in the fibre ring when the coupling strength between the orthogonal polarizations is $\kappa \approx 0.7$. The experimental results demonstrate a faithful evolution of the polarization towards the second eigenstate $|V_2\rangle$ of the system (represented by S_c and shown by a red star). The final state S_f observed in the experiment is marked by a yellow circle. **b**, Starting close to $|V_1\rangle$ but steering the system with the opposite helicity ($\gamma = 1$; CW), the polarization robustly converges to the eigenstate $|V_1\rangle$ that is located at a diametrical point on the Poincaré sphere. **c**, By keeping the helicity of encirclement as in **b** but with different initial conditions ($|V_2\rangle$), the end result remains the same: a faithful conversion towards $|V_1\rangle$—an aspect that substantiates the chirality of the process in the polarization domain. **d**–**f**, Numerical evolution of the polarization state of the system according to Supplementary equation (3) when projected on the instantaneous eigenstates. **g**–**i**, Experimentally measured polarization state projected onto the same eigenstates as in **d**–**f**. Error bars represent the uncertainty in the extraction of the Stokes parameters from the data collected by the polarimeter. The experimental trajectory in the gain-detuning parameter space is shown as an inset in **i**. Solid curves are obtained by numerically fitting the experimental data. Discrepancies between theory and experiment stem mostly from the uncertainty of the instantaneous eigenstates in the experiment (Supplementary Section 2).

quasi-adiabatic winding is satisfied (Fig. 1b). Pulses with different polarization states are launched into the system and their evolution in time is observed after each circulation in the ring. The Hamiltonian in the gain-detuning parameter space is steered in the ACW direction along an elliptical trajectory ($x_g = 2.04, x_\delta = 4.2$) that excludes the EP (yet resides in its vicinity), for a pulse initiated in a polarization state with Stokes parameters (−0.67, − 0.17, − 0.71), which is close to one of the eigenstates of the system $|V_1\rangle = (-0.78, 0.33, -0.53)$. The recorded evolution of the Stokes parameters shows to a great extent an adiabatic evolution that is intermittently disrupted by a non-adiabatic transition towards the other eigenstate $|V_2\rangle = (0.78, -0.33, 0.53)$, which is evidently the final state after 50 cycles. The trajectory of this evolution is shown in Fig. 4a. On the other hand, traversing the parametric loop in the CW direction promotes two non-adiabatic jumps that force the final polarization state to return to the initial eigenstate with Stokes parameters $|V_1\rangle = (-0.78, 0.33, -0.53)$ (Fig. 4b). As expected from theory, the two final states are indeed antipodal on the Poincaré sphere. To further verify that the system operates as a robust chiral mode convertor, we examine its response with another input polarization that happens to be closer to the complementary eigenstate $|V_2\rangle$. By initiating the process from this polarization state and letting the system evolve along the CW modulation pattern, the polarization of the pulse converges to a final state $|V_1\rangle$ after experiencing a non-adiabatic jump (Fig. 4c and Supplementary Section 2). The dynamic effects related to modulating a non-Hermitian Hamiltonian in the vicinity of an EP can be best elucidated by projecting the evolving fields $|\psi(t)\rangle$ onto the instantaneous eigenbasis at each time instant during the parametric steering process (see Supplementary Section 2). Generally, when the modulation is applied in a quasi-adiabatic manner, light tends to remain in the amplified eigenstate (with the largest imaginary part of the corresponding eigenvalue), until the followed eigenstate exchanges its amplification behaviour with the other eigenstate (halfway through the loop in Fig. 4) and the evolution becomes unstable[31]. The onset of the ensuing non-adiabatic jump is, however, delayed. The skewed vector space close to the EP helps to prompt the non-adiabatic jump. This behaviour is clearly shown in Fig. 4d–f, which shows how the population of the eigenstates changes during the encircling process without encompassing an EP. The experimental results in Fig. 4g–i further confirm that the chiral state transfer reported here is caused by the topology and shape of the Riemann surfaces and the non-orthogonality of the modes, and not necessarily by the encirclement of an EP. The width (duration) and shape of the jumps depicted in Fig. 4d–i are highly influenced by how close the trajectories are to the EP, an aspect that makes them distinctly susceptible to noise and imperfections during calibration. This may lead to new and more complex mode conversion schemes by choosing different winding paths in parameter space and/or by introducing multiple EPs.

In conclusion, we have demonstrated a multifaceted platform to study the time-resolved dynamics of parametric steering of non-Hermitian Hamiltonians. Our experimental work clearly shows that chiral mode conversion is directly related to the landscape and topology of the Riemann surfaces and the skewedness of the vector space and not necessarily to the winding around an EP, as previously thought. Our work differs from earlier demonstrations in which the analogy between time and propagation distance (z) is used to implement the necessary modulation profiles in space. In particular, the choice of polarization as a degree of freedom and our ability to map the evolution of light on the Poincaré sphere after each round trip allow us to uniquely and with great precision expose the peculiarities of dynamical non-Hermitian systems in time. Our work may open new vistas in understanding the chiral and topological behaviours in non-Hermitian arrangements and can be used to develop a more comprehensive formalism for the adiabatic theorem in slowly varying non-Hermitian systems.

Online content

Any methods, additional references, Nature Research reporting summaries, source data, extended data, supplementary information, acknowledgements, peer review information; details of author contributions and competing interests; and statements of data and code availability are available at https://doi.org/10.1038/s41586-022-04542-2.

1. Uzdin, R., Mailybaev, A. & Moiseyev, N. On the observability and asymmetry of adiabatic state flips generated by exceptional points. *J. Phys. A* **44**, 435302 (2011).
2. Graefe, E.-M., Mailybaev, A. A. & Moiseyev, N. Breakdown of adiabatic transfer of light in waveguides in the presence of absorption. *Phys. Rev. A* **88**, 033842 (2013).
3. Gilary, I., Mailybaev, A. A. & Moiseyev, N. Time-asymmetric quantum-state-exchange mechanism. *Phys. Rev. A* **88**, 010102 (2013).
4. Doppler, J. et al. Dynamically encircling an exceptional point for asymmetric mode switching. *Nature* **537**, 76–79 (2016).
5. Xu, H., Mason, D., Jiang, L. & Harris, J. G. Topological energy transfer in an optomechanical system with exceptional points. *Nature* **537**, 80–83 (2016).
6. Yoon, J. W. et al. Time-asymmetric loop around an exceptional point over the full optical communications band. *Nature* **562**, 86–90 (2018).
7. Hassan, A. U., Zhen, B., Soljačić, M., Khajavikhan, M. & Christodoulides, D. N. Dynamically encircling exceptional points: exact evolution and polarization state conversion. *Phys. Rev. Lett.* **118**, 093002 (2017).
8. Zhang, X.-L. & Chan, C. T. Dynamically encircling exceptional points in a three-mode waveguide system. *Commun. Phys.* **2**, 63 (2019).
9. Hassan, A. U. et al. Chiral state conversion without encircling an exceptional point. *Phys. Rev. A* **96**, 052129 (2017).
10. Zhong, Q., Khajavikhan, M., Christodoulides, D. N. & El-Ganainy, R. Winding around non-Hermitian singularities. *Nat. Commun.* **9**, 4808 (2018).
11. Feilhauer, J. et al. Encircling exceptional points as a non-Hermitian extension of rapid adiabatic passage. *Phys. Rev. A* **102**, 040201 (2020).
12. Kato, T. *Perturbation Theory for Linear Operators* (Springer, 2013).
13. Heiss, W. D. Phases of wave functions and level repulsion. *Eur. Phys. J. D* **7**, 1–4 (1999).
14. Moiseyev, N. *Non-Hermitian Quantum Mechanics* (Cambridge Univ. Press, 2011).
15. El-Ganainy, R. et al. Non-Hermitian physics and PT symmetry. *Nat. Phys.* **14**, 11–19 (2018).
16. Parto, M., Liu, Y. G. N., Bahari, B., Khajavikhan, M. & Christodoulides, D. N. Non-Hermitian and topological photonics: optics at an exceptional point. *Nanophotonics* **10**, 403–423 (2021).
17. Makris, K. G., El-Ganainy, R., Christodoulides, D. N. & Musslimani, Z. H. Beam dynamics in PT symmetric optical lattices. *Phys. Rev. Lett.* **100**, 103904 (2008).
18. Klaiman, S., Günther, U. & Moiseyev, N. Visualization of branch points in PT-symmetric waveguides. *Phys. Rev. Lett.* **101**, 080402 (2008).
19. Zheng, M. C., Christodoulides, D. N., Fleischmann, R. & Kottos, T. *PT* optical lattices and universality in beam dynamics. *Phys. Rev. A* **82**, 010103 (2010).
20. Milburn, T. J. et al. General description of quasiadiabatic dynamical phenomena near exceptional points. *Phys. Rev. A* **92**, 052124 (2015).
21. Zhang, X.-L., Wang, S., Hou, B. & Chan, C. T. Dynamically encircling exceptional points: in situ control of encircling loops and the role of the starting point. *Phys. Rev. X* **8**, 021066 (2018).
22. Zhang, X.-L., Jiang, T. & Chan, C. T. Dynamically encircling an exceptional point in anti-parity-time symmetric systems: asymmetric mode switching for symmetry-broken modes. *Light Sci. Appl.* **8**, 88 (2019).
23. Choi, Y., Hahn, C., Yoon, J. W., Song, S. H. & Berini, P. Extremely broadband, on-chip optical nonreciprocity enabled by mimicking nonlinear anti-adiabatic quantum jumps near exceptional points. *Nat. Commun.* **8**, 14154 (2017).
24. Choi, Y., Yoon, J. W., Hong, J. K., Ryu, Y. & Song, S. H. Direct observation of time-asymmetric breakdown of the standard adiabaticity around an exceptional point. *Commun. Phys.* **3**, 140 (2020).
25. Gao, T. et al. Observation of non-Hermitian degeneracies in a chaotic exciton-polariton billiard. *Nature* **526**, 554–558 (2015).
26. Dembowski, C. et al. Experimental observation of the topological structure of exceptional points. *Phys. Rev. Lett.* **86**, 787 (2001).
27. Mailybaev, A. A., Kirillov, O. N. & Seyranian, A. P. Geometric phase around exceptional points. *Phys. Rev. A* **72**, 014104 (2005).
28. Heiss, W. D. The physics of exceptional points. *J. Phys. A* **45**, 444016 (2012).
29. Dembowski, C. et al. Encircling an exceptional point. *Phys. Rev. E* **69**, 056216 (2004).
30. Liu, Q., Liu, J., Zhao, D. & Wang, B. On-chip experiment for chiral mode transfer without enclosing an exceptional point. *Phys. Rev. A* **103**, 023531 (2021).
31. Berry, M. V. & Uzdin, R. Slow non-Hermitian cycling: exact solutions and the Stokes phenomenon. *J. Phys. A* **44**, 435303 (2011).

Methods

In our setup, shown in Fig. 2b, a 330-ns laser pulse at a wavelength of 1,547 nm (generated by a semiconductor laser and an intensity modulator) featuring an arbitrary state of polarization is injected into the main loop through a 3-dB coupler. The single-mode fibre in use is not polarization maintaining. Here we refer to the two orthogonal polarization states as P_1 and P_2. A two-dimensional parameter space is formed through the gain and detuning (phase difference between P_1 and P_2). A polarization beamsplitter directs the vertical and horizontal field components into two separate branches where they independently yet simultaneously experience gain and phase modulation, imposed by electro-optic intensity and phase modulators, respectively, with a temporal dependence as described in equation (2). The branches are equalized in terms of their length and insertion loss by deploying a variable optical attenuator and a delay line. The two beams are then combined by means of a polarization beam combiner. Finally, a constant coupling is provided by a polarization controller that mixes the polarization states. At the end of each round trip, half of the pulse couples out of the fibre ring for monitoring purposes and the rest remains in the loop to repeat the process (with the modulation patterns stated in equation (2)), until the desired number of pulse circulations is attained. The part of the pulse that exits the loop in each cycle provides a unique opportunity for in situ and real-time monitoring of the light's polarization evolution during the encirclement process. In this setup, the degree of adiabaticity can be controlled with the aid of two acousto-optic modulators that gate pulse circulation and therefore set the desired encirclement time. To prevent pulses from fading, an erbium-doped fibre amplifier is inserted in the loop, to compensate the insertion loss introduced by the electro-optics and fibre components (Supplementary Section 3). In the ring, a 300-m-long single-mode fibre ensures the presence of only one pulse during the total encirclement process (91.5 μs). Each round trip lasts approximately 1.83 μs. The polarimeter used in this study (NOVOPTEL PM1000) has a sampling rate of 100 MHz that allows one to properly characterize pulses with a duration of 330 ns.

Data availability

All data that support the findings of this study are available within the paper and the Supplementary Information and are available from the corresponding author upon request.

Acknowledgements We gratefully acknowledge the financial support from the Air Force Office of Scientific Research (Multidisciplinary University Research Initiative (MURI) Award on Novel light-matter interactions in topologically non-trivial Weyl semimetal structures and systems: FA9550-20-1-0322, MURI Award on Programmable systems with non-Hermitian quantum dynamics: FA9550-21-1-0202), DARPA (D18AP00058), the Office of Naval Research (N00014-19-1-2052, N00014-20-1-2522, MURI Award on Classical entanglement in structured optical fields: N00014-20-1-2789), the Army Research Office (W911NF-17-1-0481), the National Science Foundation (DMR-1420620, EECS-1711230, ECCS CBET 1805200, ECCS 2000538, ECCS 2011171), the W. M. Keck Foundation, the US–Israel Binational Science Foundation (BSF; 2016381), the MPS Simons collaboration (Simons grant 733682), the US Air Force Research Laboratory (FA86511820019), the Austrian Science Fund (FWF, P32300 WAVELAND) and European Commission grant MSCA-RISE 691209. G.L-G. acknowledges support from Consejo Nacional de Ciencia y Tecnologia (CONACyT). We thank A. Turchanin and U. Peschel from Friedrich Schiller University Jena for useful discussions and feedback.

Author contributions D.N.C. and M.K. conceived the idea. H.N., G.L.-G. and H.E.L.-A. designed and performed the experiments in consultation with other team members. H.N., A.U.H. and A.S. performed the analysis with help from other members. H.N., M.K. and D.N.C. wrote the manuscript with help from all the authors.

Competing interests The authors declare no competing interests.

Additional information
Supplementary information The online version contains supplementary material available at https://doi.org/10.1038/s41586-022-04542-2.
Correspondence and requests for materials should be addressed to Mercedeh Khajavikhan.
Peer review information *Nature* thanks Jae Woong Yoon and the other, anonymous, reviewer(s) for their contribution to the peer review of this work.
Reprints and permissions information is available at http://www.nature.com/reprints.